Los Alamos National Laboratory is operated by the University of California for the United States Department of Energy under contract W-7405-ENG-36.

Reverse Vortex Flow in Near-Surface Explosions

Los Alamos National Laboratory
Los Alamos, New Mexico 87545

This work was supported, in part, by the Defense Nuclear Agency.

LA-8947-MS

UC-35
Issued: September 1981

Reverse Vortex Flow in Near-Surface Explosions

Eric M. Jones
Rodney W. Whitaker

Los Alamos National Laboratory
Los Alamos, New Mexico 87545

REVERSE VORTEX FLOW IN NEAR-SURFACE EXPLOSIONS

by

Eric M. Jones and Rodney W. Whitaker

ABSTRACT

Nuclear explosions conducted near the ground surface but higher than about 5-6 $m/kt^{1/3}$ produce a reverse flow (downward along the symmetry axis) after the shock wave is reflected from the ground. This reverse flow persists until destroyed by the buoyant rise of the fireball on time scales of several seconds.

Six calculations of bursts with scaled heights-of-burst ranging upward from 15 $m/kt^{1/3}$ are described. The height of the reverse flow is a simple function of the burst height and explosion yield.

I. INTRODUCTION

For some years it has been known that atmospheric nuclear explosions conducted at scaled heights-of-burst (SHOB) of the order of 30 $m/kt^{1/3}$ produce strong reverse flow below the fireball. In particular, downward flow of air directly over surface-ground-zero (SGZ) may delay the time when soil and dust are swept into the nuclear cloud. The effect was first noticed in HULL-code calculations.* Confirming photographic evidence has been found for Upshot-Knothole BADGER and HARRY.

In this report we will briefly describe generation of the reverse flow, conditions necessary for its existence, the extent of the region of downward motion above SGZ, and comparisons with a limited amount of data.

---

* The reverse flow was called to our attention in 1975-1976 by D. H. Dean and P. S. Lewis, Jr. of McDonnell Douglas Astronautics Company and by C. Needham, then at the Air Force Weapons Laboratory. These groups had independently encountered the reverse flow phenomenon in Hull code calculations.

II. GENERATION OF THE REVERSE FLOW

The reverse flow is produced as a result of the reflection of a strong nuclear shock wave from the ground surface. Consequently, the reverse flow appears only if the SHOB falls in a restricted altitude regime. At the low end of the range the reverse flow will not occur if the explosion is close enough to the surface that a shock wave is not formed by the time the fireball interacts with the ground. At the upper end, shock waves produced by bursts at relatively high altitudes are sufficiently weak that no sensible reverse flow is generated.

Let us first consider the minimum height-of-burst for which the reverse flow occurs and then describe the generation of a typical flow at higher altitude.

An atmospheric nuclear explosion deposits energy in the air by three mechanisms: deposition of x rays produced by the high temperature of the weapon case, deposition of neutrons, and collision of the rapidly expanding weapon debris with the air molecules. Because the mean free path of neutrons in sea-level air is of the order of a hundred meters, they have relatively little effect on the formation of the reverse vortex and will not be considered further.

A fireball generated primarily by x-ray deposition grows radiatively until such time as the time scale for propagation of the radiation front becomes comparable with hydrodynamic time scales and a hydrodynamic shock wave forms.

In the case of an x-ray fireball, the hydrodynamic shock forms at a radius of

$$R_{sh} = 5.5\ (Y/\rho_o)^{1/3}\ \text{m}\ ,$$

where Y is the explosion energy in kilotons and ρ_o is the ambient air density in milligrams per cubic centimeter. The above scaling is based on fits to RADFLO calculations. The precise value of the coefficient will depend on the fraction of the yield radiated in x rays.

If, on the other hand, the fraction of the device energy in x rays is low, there may be no radiative growth phase. In this case a strong hydrodynamic shock will have formed in air by the time that a mass of air about equivalent to the weapon mass has been entrained by the expanding debris.

For the case of the explosion of a massive device with no x-ray emission, the radius at which a bomb mass of air is entrained and at which the flow field approaches the classical blast wave solution is

$$R_{bw} = 6.2\ (M/\rho_o)^{1/3} \quad ,$$

where M is the mass of the device in metric tonnes. For most modern devices the mass-to-yield ratio is low and the x-ray output significant so there will be a radiative phase and the reverse flow will occur only for explosions at SHOB larger than 5-6 m.

For explosions higher than 5-6 $m/kt^{1/3}$, a shock wave forms. As it strikes the ground the pressure at SGZ rises to high values and a stronger reflected shock wave moves back toward the burst point. Initially, material behind the reflected shock moves upward, lowering the pressure and density at SGZ, and creating a positive pressure gradient; i.e., in the region near SGZ when the lowest pressure is at SGZ. The pressure gradient decelerates the upward flow and eventually reverses it. Two-dimensional effects lead to rotational flows that form the reverse vortex. Transients in the flow lead to oscillation in the size and rotational speed of the reverse vortex.

The fireball itself, the volume of hot low density air created by the explosion, is buoyant and is accelerated upward at about 2 g. For most nuclear events significant buoyant motions occur on time scales of seconds or tens of seconds. Once the buoyant motion is established, the general upward flow of material induced beneath the rising fireball breaks up the reverse vortex.

III. A DETAILED NUMERICAL CALCULATION - BADGER

Upshot-Knothole BADGER was a 23-kt nuclear explosion conducted on a 91-m tower at the Nevada Test Site on April 18, 1953. The BADGER device was closely surrounded by a considerable mass of shielding, tower structure, etc; but by 10 ms, when the shock struck SGZ, the shock was well formed and moving at Mach 11.

The flow at 20 ms is illustrated in Fig. 1. Particularly striking is the distribution of pressure showing the main shock, the well-developed Mach stem, the reflected shock wave, and the developing pressure gradient above SGZ.

By 25 ms the positive gradient is well established, and there are clear signs of deceleration of the material above SGZ (Fig. 2).

By 50 ms the reverse flow is established. However, as can be seen in the pressure distribution (Fig. 3), the pressure at SGZ is rising, indicative of the transients that persist in the flow.

Figure 4 is a sequence of velocity profiles along the symmetry axis showing the development of the reverse flow. The first negative velocities occur at about 38 ms about 10 m above SGZ. Although the reverse flow shows oscillation in spatial extent and in flow speeds, the overall reverse flow grows with time. By 0.4 s the largest on-axis downward velocity is about 260 m/s and the downward flow covers the entire region between SGZ and 120-m altitude. Thereafter the largest negative velocity begins to decline in magnitude, although the height of the reverse flow increases to 210 m at 1.7 s before beginning to decrease.

As indicated above, the decay of the reverse flow seems to correspond to the beginning of buoyant rise of the fireball. For BADGER, a characteristic fireball radius is 40 m and a characteristic buoyancy time, the time for the fireall to rise its own radius at 2 g, is $t_b = \sqrt{R/g}$ = 2.0 s. By 5.8 s the reverse flow has dissipated.

IV. HEIGHT OF THE REVERSE FLOW

We have performed six radiation transport/hydrodynamics calculations of atmospheric nuclear explosions. Three are of 540-kt explosions at burst heights of 124, 248, and 450 m (KING). The others are of GRABLE (15 kt at 160 m), HARRY (32 kt at 61 m), and BADGER (23 kt at 91 m). The SHOB range from 15.4 m/kt$^{1/3}$ for the lowest of the 540-kt explosions to 65 m/kt$^{1/3}$ for GRABLE.

We have found that the vertical extent of the reverse flow region is a well-behaved function of the height-of-burst and the yield. In particular we have determined from the computer output the height of the velocity reversal point on axis - the altitude at which the velocity goes from negative in the reverse flow to positive in the flow behind the reflected shock wave. We note that during the interval before formation of the reflected shock and the reverse vortex

there is a reversal point near the burst point. However, this corresponds to the flow outward from the center before the arrival of the reflected shock at the fireball center. We have carefully distinguished between the two types of flow reversal.

Figure 5 shows the scaled height of the reversal point as a function of scaled time for the three 540-kt calculations. The other three calculations are presented in Fig. 6. Note that we have also plotted the height of the bottom of the reverse flow. There are occasions when there is a small region of upward motion just above SGZ. This is clearly related to the oscillatory behavior of the reverse flow described above. These occurrences of positive motion correspond closely to the times of smallest vertical extent of the oscillating reverse vortex.

The dominant feature of Figs. 5 and 6 is that the upper envelopes to the vortex heights define a well-behaved family of curves:

$$Z/HOB = \log (t/W^{1/3}) + 3.53 - 0.035 (HOB/W^{1/3}) \quad ,$$

where Z is the height (in meters) of the top of the reverse vortex as a function of time (t). HOB is the height-of-burst in meters, and W is the yield in kilotons. The family of curves is illustrated in Fig. 7.

In an effort to assess the validity of our calculations, we requested that trajectories be measured for clumps of material in the BADGER cloud. These measurements were performed by J. Colvin of EG&G-LAO. In Fig. 8 we compare the trajectories for three clumps determined in the interval 0.4-0.5 s with the flow field at 0.45 s as determined in the calculations. Three of the four show qualitative argeement. There is disagreement between the calculated flow field and the motion of the fourth clump. In Fig. 9 we make similar comparisons at about 1.3 s with good agreement. The overall agreement is encouraging, but we note that the BADGER fireball is very irregular and turbulent. This may explain the deviation of the one clump at half a second but also necessitates extreme caution in interpreting BADGER.

As indicated earlier, the overall growth of the reverse vortex ends as the fireball begins its buoyant rise. From the data in Figs. 5 and 6, we estimate that the reverse vortex disappears at a time of $3.5\ W^{1/6}$ s. However, we note

that in all the calculations the resolution in the reverse vortex is poor at these late times and, therefore, we urge caution in using this estimate.

We have examined photographic records in a effort to better define the times at which the reverse vortex disappears. The reverse flow is most prominent in records of Upshot—Knothole HARRY and BADGER. However, owing to the large amounts of mass near the BADGER and HARRY devices and to the considerable dust and smoke raised by the shock, the photographic records of these events are difficult to interpret for the disappearance of the reverse vortex. The film records show that material that had been in the upper part of the reverse flow began to rise at 3.8 s for HARRY and 4.8 s for BADGER. It is entirely possible that downward flow persisted close to SGZ for somewhat longer times but the considerable obscuration makes any definitive statement impossible. The 4.8-s time observed for BADGER corresponds to the time the calculated reverse vortex height had dropped to 40 m. We consider the estimate of 3.5 $W^{1/6}$ s for disappearance of the flow to be plausible. Any error is not likely to be large.

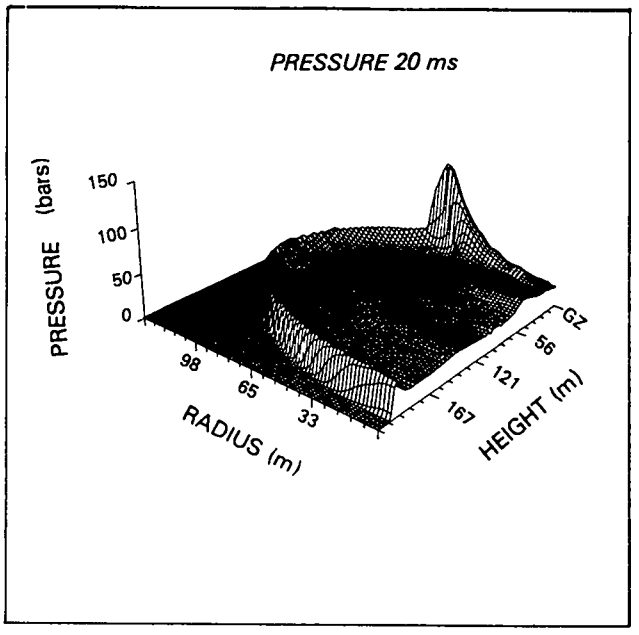

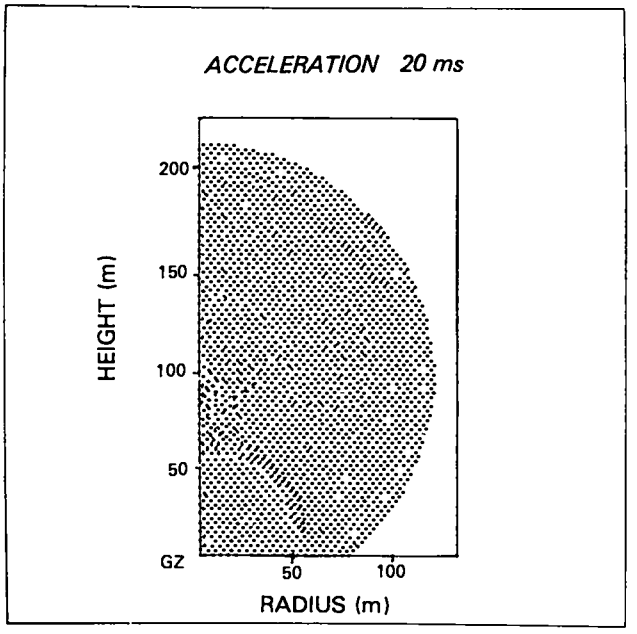

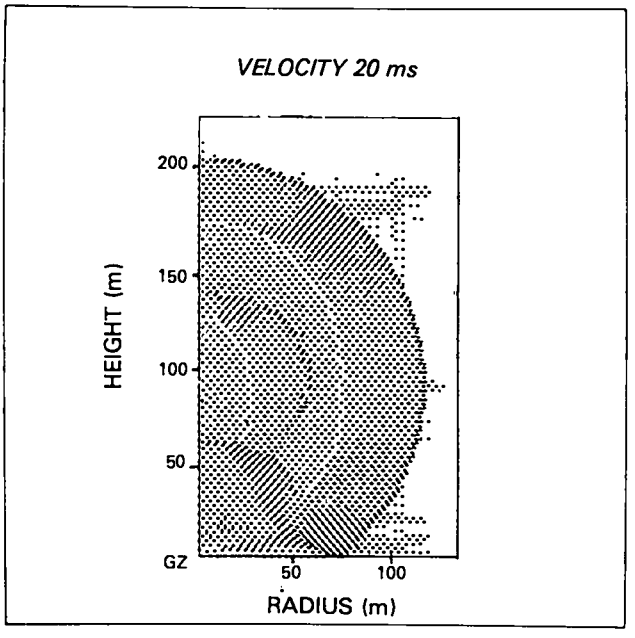

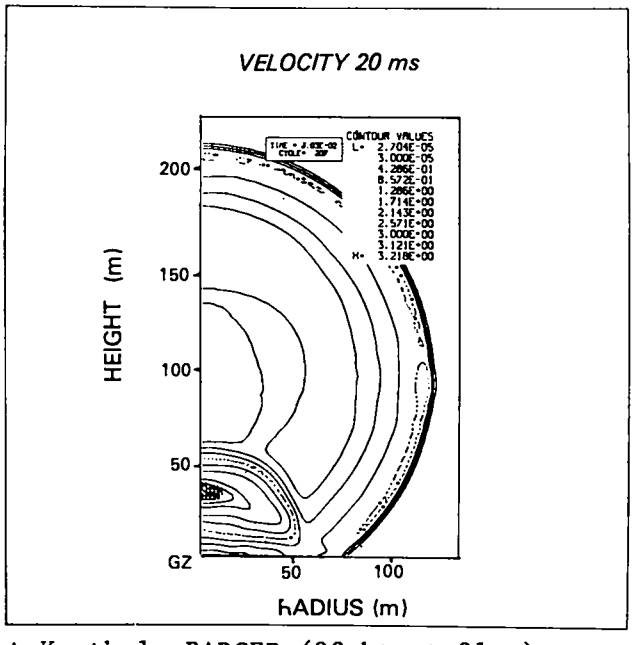

Figure 1. Flow field calculated for Upshot-Knothole BADGER (23 kt at 91 m) at 20 ms. The flow is characterized by the direct shock that has reached a radius of 120 m, the reflected shock that has reached 60-m altitude on the vertical axis, and their intersection, which is particularly prominent at about 75-m radius in the pressure plot. The expanding, spherical disturbance with a radius of about 40 m and centered on the burst point is real and can be seen in one-dimensional calculations.

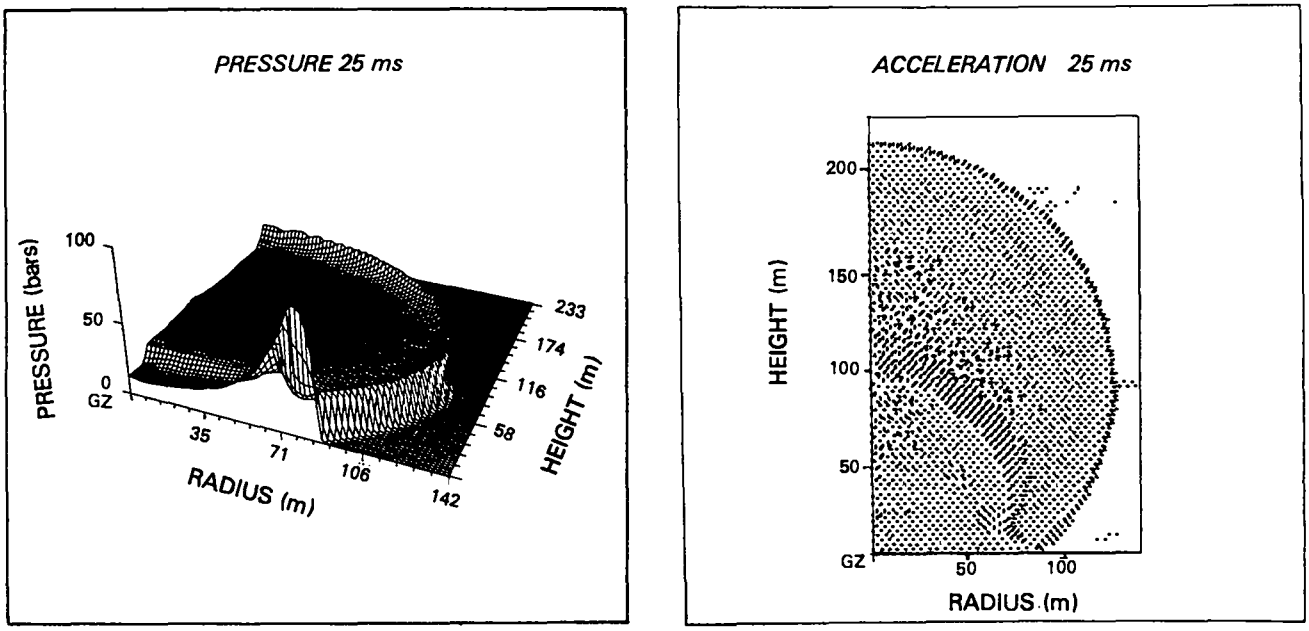

Figure 2. Badger at 25 ms. A rarefaction at ground zero (GZ) has lowered the pressure and created a strong positive pressure gradient at about 25-m altitude. The downward accelerations generated by this gradient are the source of the reverse vortex. Note the reflected shock in the acceleration plot, having reached 110-m altitude on axis.

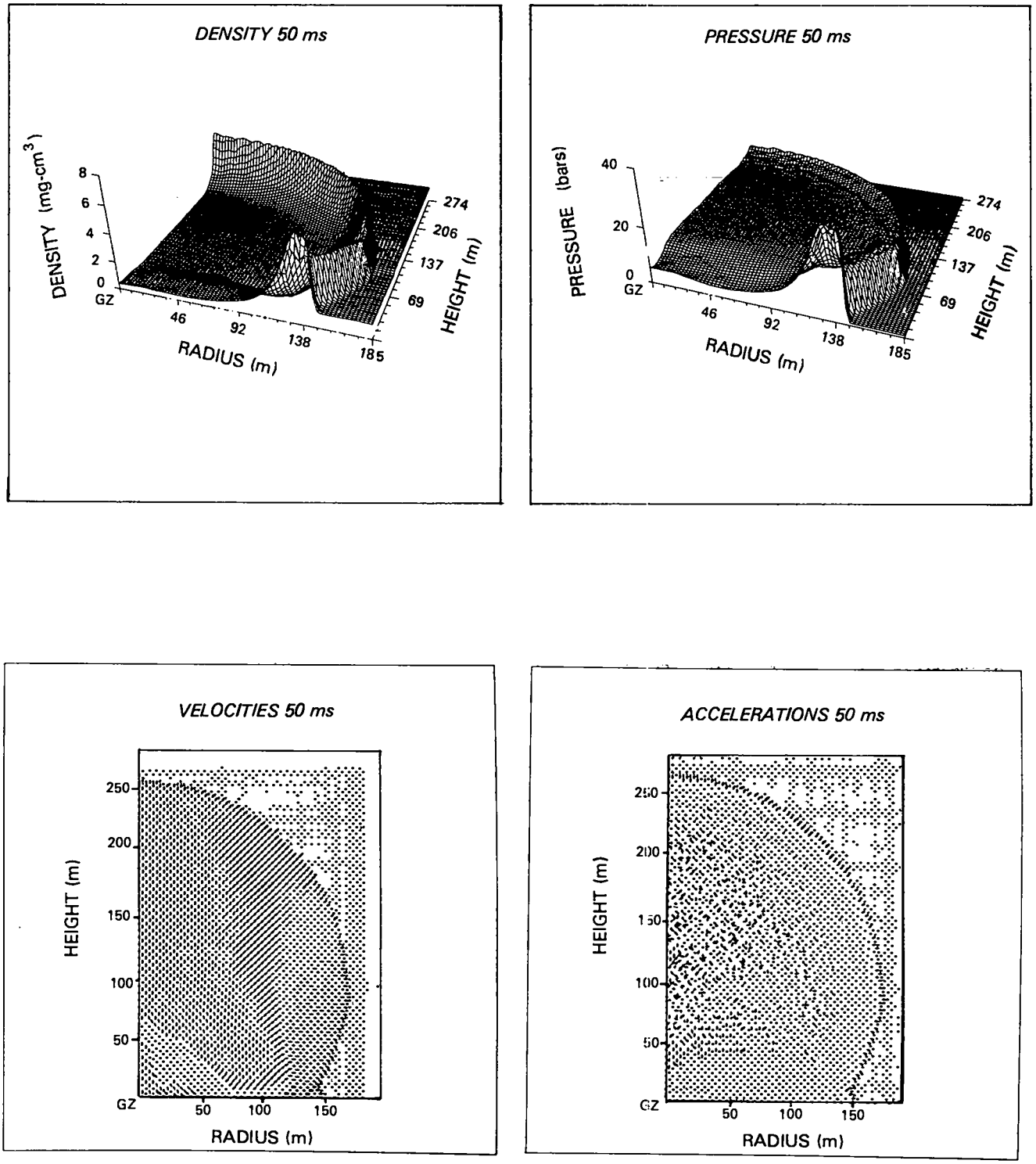

Figure 3. BADGER at 50 ms. The reverse flow is established. Note the counter-clockwise flow is the region within 50 m of GZ. Note in the pressure plot (upper right) that the pressure at GZ has risen, creating a negative gradient. This is an indication of the real transients in the flow.

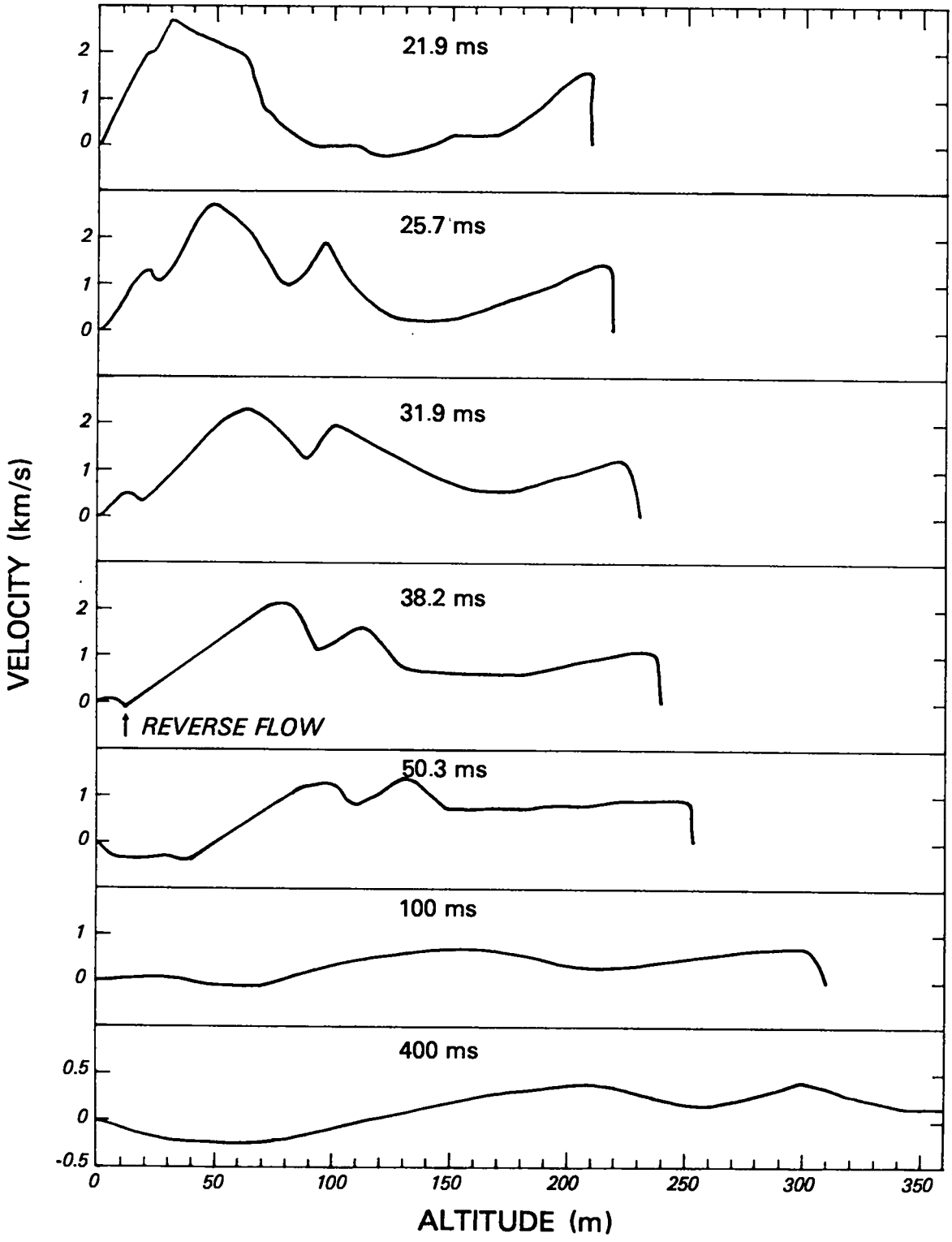

Figure 4. On-axis velocity profiles for BADGER. The reverse flow first appears at 38 ms at about 15-m altitude. Note that at 100 ms there is a region of upward flow for about 30-40 m above GZ. At 400 ms the reverse flow is re-established.

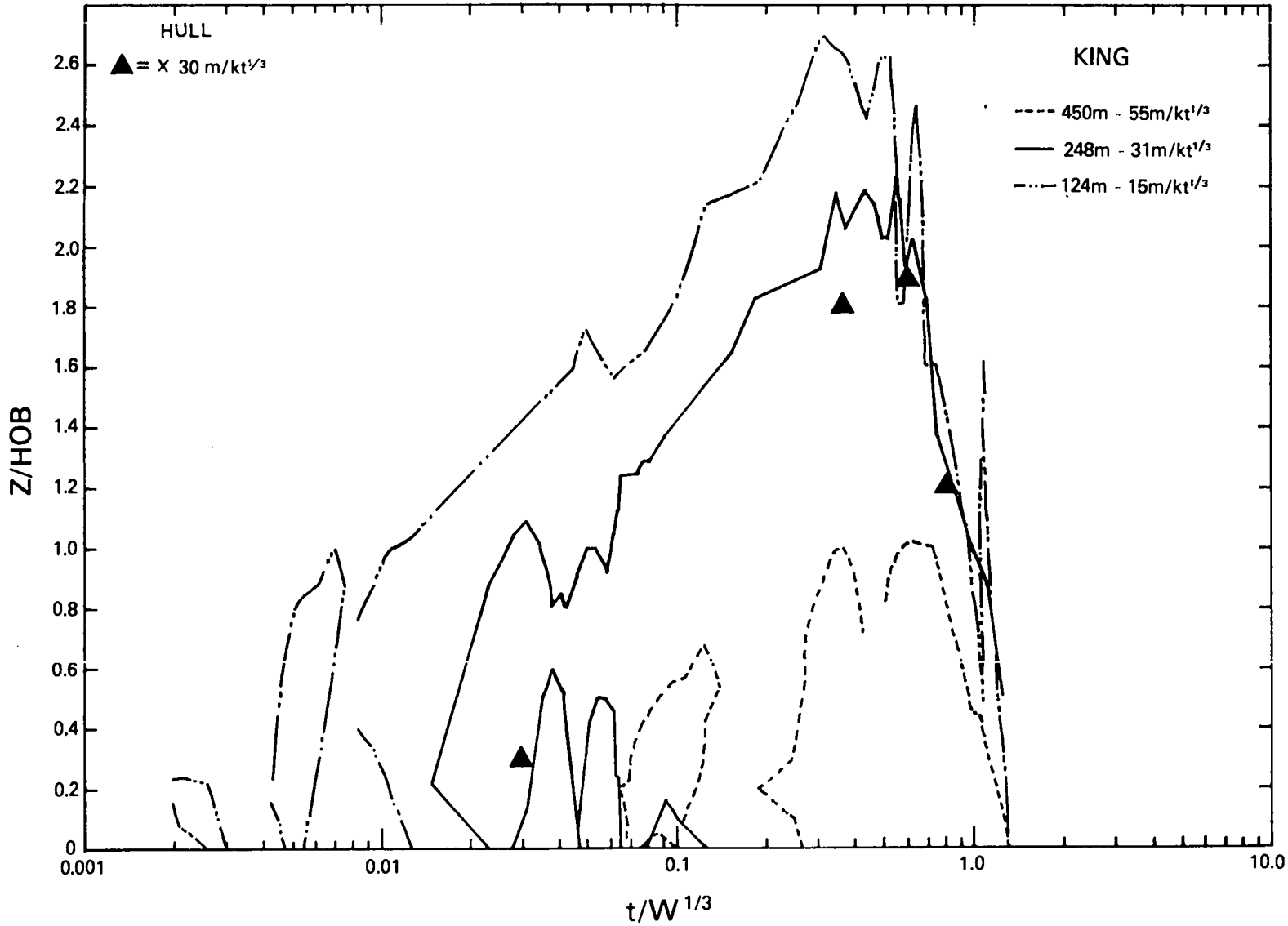

Figure 5. Boundaries of the reverse vortex on the vertical axis. These three calculations each had a yield of 540 kt (the IVY-KING yield). Notice that during the early phases the bottom of the vortex might be above GZ. At later times the vortex extends to the ground surface.

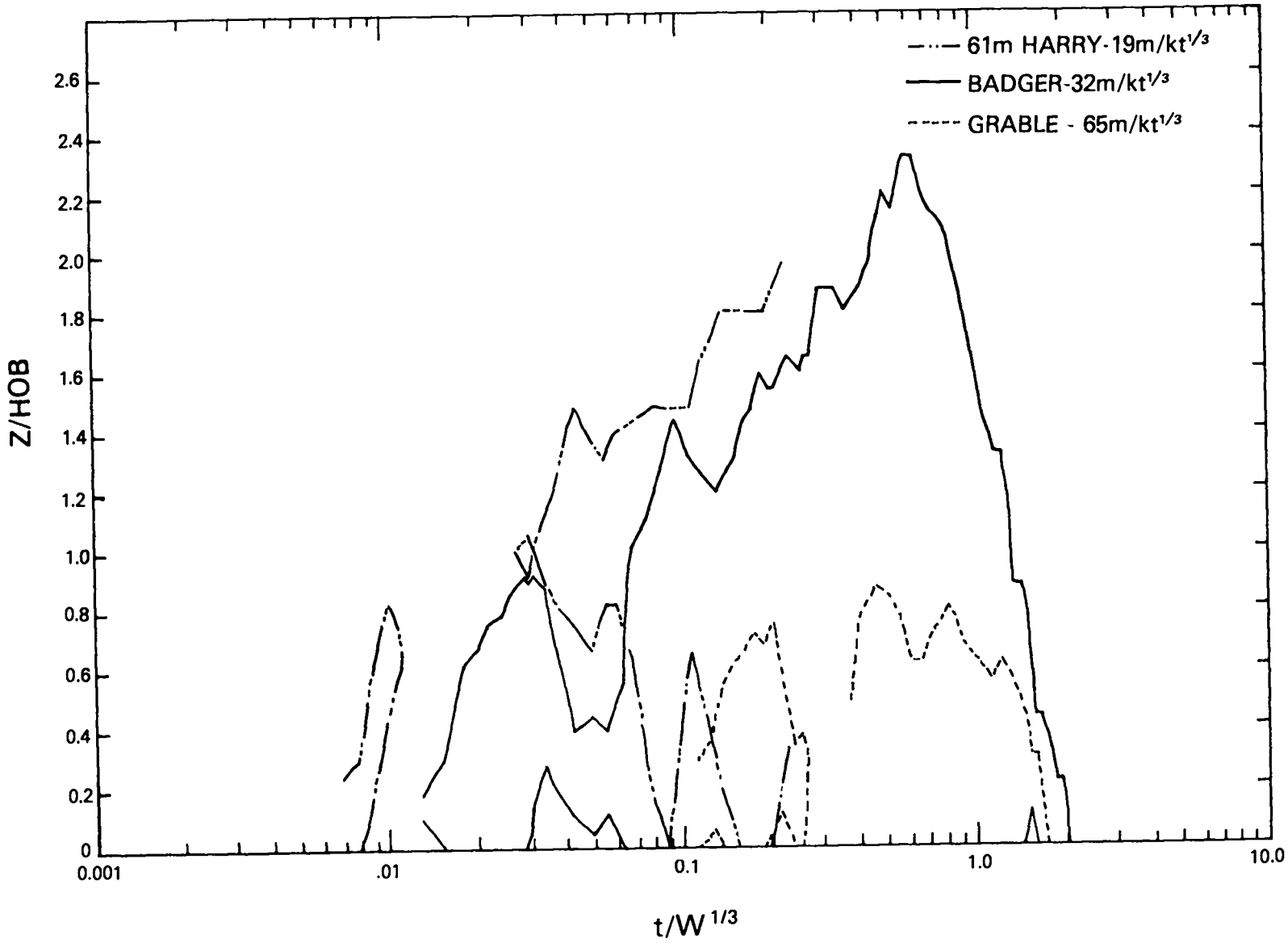

Figure 6. Extent of the reverse flow for three additional calculations.

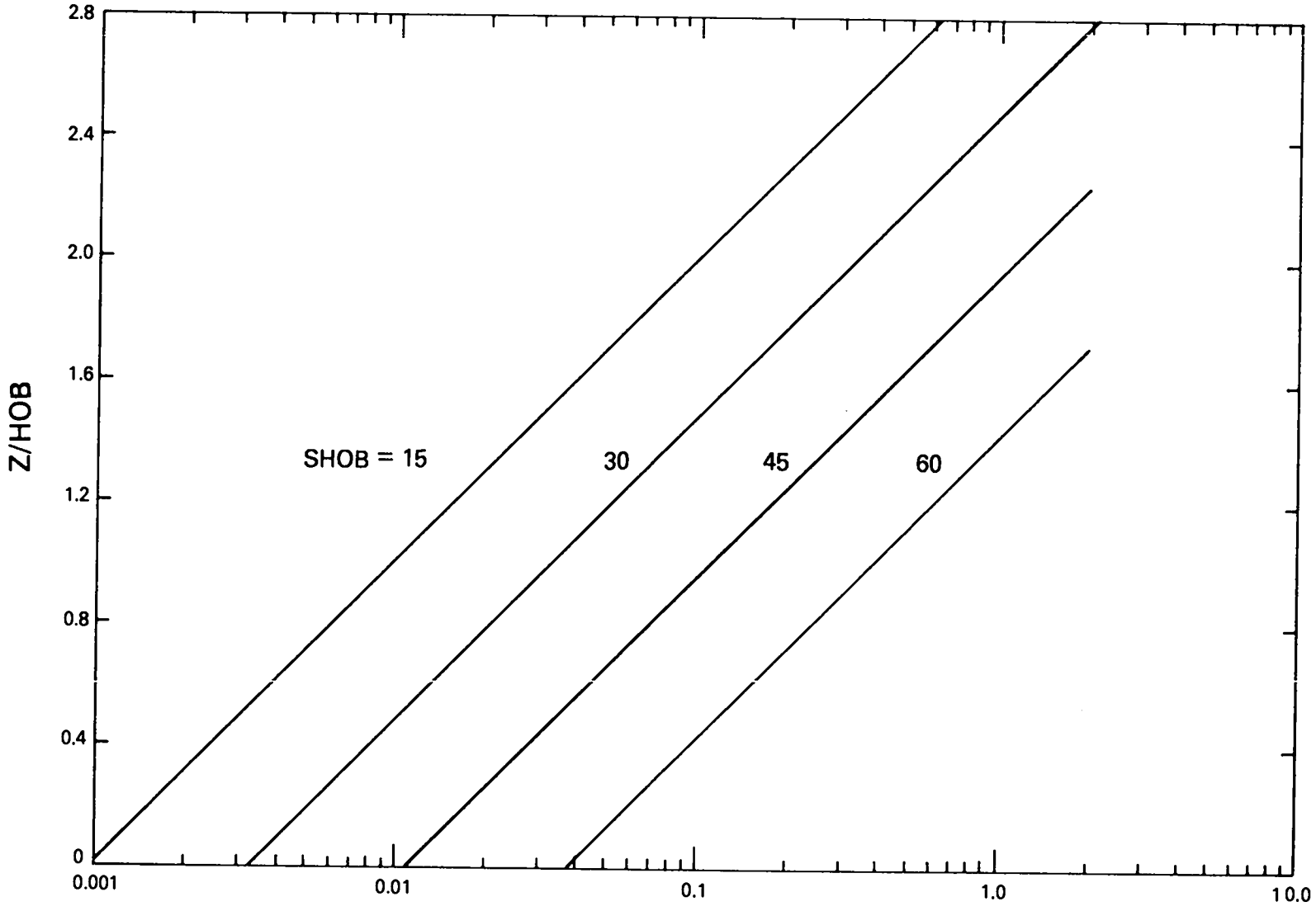

Figure 7. This family of curves represent upper envelopes to the maximum height of the reverse flow on the axis as a function of scaled time ($sec/kt^{1/3}$). The curves are labelled with the appropriate scaled height-of-burst ($SHOB = HOB/W^{1/3}$).

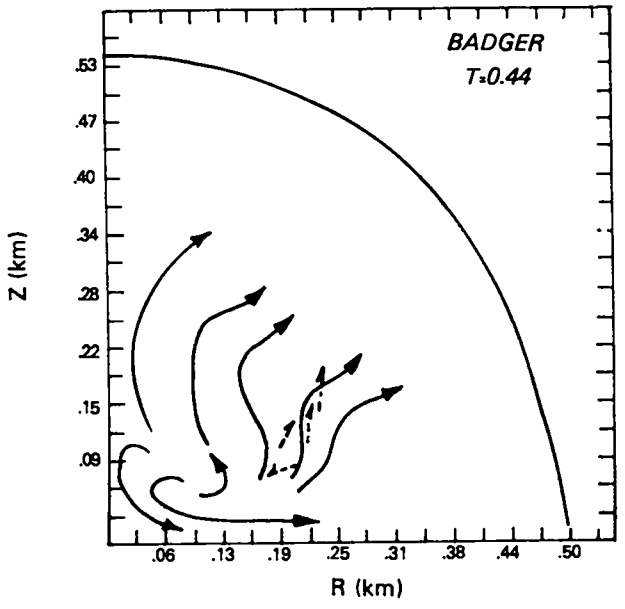

Figure 8. Streamlines for BADGER at 0.44 s compared with photographically determined clump motions. There is general agreement except for the lowermost clump (see text for discussion).

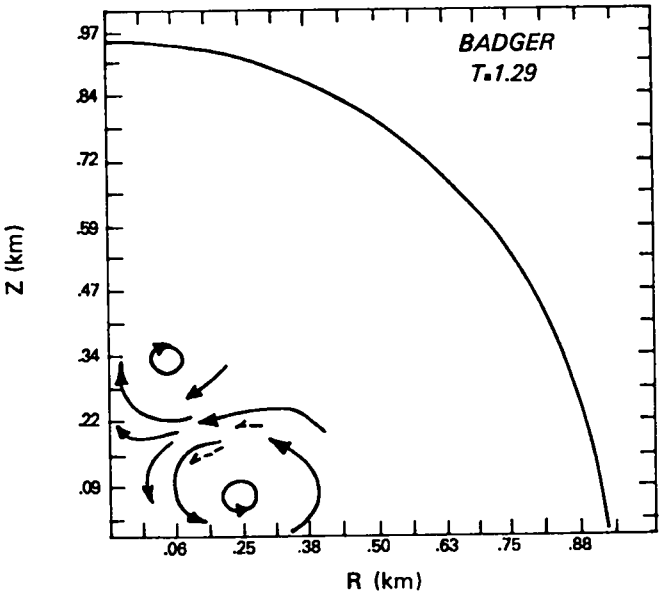

Figure 9. Streamlines for BADGER at 1.29 s compared with photographically determined clump motions.

Printed in the United States of America
Available from
National Technical Information Service
US Department of Commerce
5285 Port Royal Road
Springfield, VA 22161

Microfiche $3.50 (A01)

Page Range	Domestic Price	NTIS Price Code	Page Range	Domestic Price	NTIS Price Code	Page Range	Domestic Price	NTIS Price Code	Page Range	Domestic Price	NTIS Price Code
001-025	$ 5.00	A02	151-175	$11.00	A08	301-325	$17.00	A14	451-475	$23.00	A20
026-050	6.00	A03	176-200	12.00	A09	326-350	18.00	A15	476-500	24.00	A21
051-075	7.00	A04	201-225	13.00	A10	351-375	19.00	A16	501-525	25.00	A22
076-100	8.00	A05	226-250	14.00	A11	376-400	20.00	A17	526-550	26.00	A23
101-125	9.00	A06	251-275	15.00	A12	401-425	21.00	A18	551-575	27.00	A24
126-150	10.00	A07	276-300	16.00	A13	426-450	22.00	A19	576-600	28.00	A25
									601-up	†	A99

†Add $1.00 for each additional 25-page increment or portion thereof from 601 pages up.